



Article

pubs.acs.org/IECR

# Selective Catalytic Reduction of Nitric Oxide by Ammonia over V<sub>2</sub>O<sub>5</sub>/TiO<sub>2</sub> in a Hollow Cylindrical Catalyst under Enhancing Effect of Electrohydrodynamics: A Kinetic Modeling Study

Milad Nahavandi\*

Department of Chemical Engineering, Isfahan University of Technology, Isfahan 84156-83111, Iran

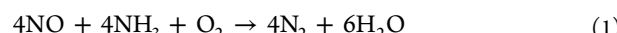
**ABSTRACT:** Emissions of nitrogen oxides (NO<sub>x</sub>) in fuel combustion from stationary and mobile sources contribute to the greenhouse effects and cause a variety of environmentally harmful results. Meanwhile, the selective catalytic reduction (SCR) of NO<sub>x</sub> using ammonia over a vanadia-based catalyst in heterogeneous reactors is still a well-proven technique for NO<sub>x</sub> abatement. However, to meet forthcoming restrictive legislation, greater De-NO<sub>x</sub> performance can be achieved by eliminating operational setbacks such as diffusion resistance, poor catalyst activity at low temperatures, etc. In this study, an electrohydrodynamic (EHD)-SCR model was developed to evaluate the enhancing effect of the EHD technique on NH<sub>3</sub>-SCR of NO through a hollow cylindrical catalyst. Computational investigations were performed based on the proposed model in different operational conditions to examine the effect of various operating parameters on SCR enhancement. Simulation results showed that catalyst utilization was intensified significantly by EHD application and generation of additional flow known as EHD-induced secondary flow through the catalyst porous layer, which undermined the proposed drawbacks of the catalyst medium and provided higher catalyst effectiveness with greater NO conversion. Results also indicated that the maximum enhancement of almost 4.2-fold could be obtained for NO conversion with electric potentials and operating temperatures of 150–270 V and 150–165 °C, respectively.

## 1. INTRODUCTION

In recent decades, the concentration of anthropogenic pollutants in the atmosphere has increased rapidly and the problem of air pollution, especially emissions of nitrogen oxides (NO<sub>x</sub>) in fuel combustion from stationary and mobile sources, has become ecologically serious as they cause a variety of environmentally harmful effects such as acid rain and urban smog and contribute to the greenhouse effects along with CO<sub>2</sub>, CH<sub>4</sub>, and H<sub>2</sub>O. Therefore, the abatement of NO<sub>x</sub> has become an important concern of industrialized countries, and great efforts have been focused on development of technologies to reduce NO<sub>x</sub> emission.<sup>1</sup>

Heterogeneous catalysis is used widely in chemical, refinery, and particularly in pollution control processes, including reduction of toxic emissions such as NO<sub>x</sub>. The technique of decomposing NO<sub>x</sub> with the selective catalytic reduction (SCR) of NO by NH<sub>3</sub> (NH<sub>3</sub>-SCR) over a vanadia-based catalyst is one of the most efficient methods. This technique, which was established in the 1970s, is still a major strategy for reduction of NO<sub>x</sub> industrially.<sup>2</sup> NH<sub>3</sub>-SCR has been used mainly for stationary sources because of its high efficiency and the ability of ammonia to react selectively with NO<sub>x</sub> to form N<sub>2</sub> and its resistance to the poisoning and aging of applied catalysts.<sup>3</sup> This technique is also being employed more and more to reduce NO<sub>x</sub> in exhaust gases of internal combustion engines operating with excess air, such as diesel engines installed in heavy-duty vehicles and passenger cars. NH<sub>3</sub>-SCR is based on the reaction between NO<sub>x</sub> and NH<sub>3</sub> to produce water and nitrogen, which can be described by a reaction network that involves two parallel reactions. The desired reaction is the conversion of NO to N<sub>2</sub> according to eq 1, while the oxidation of ammonia given in eq 2 is an undesired reaction during NO<sub>x</sub> destruction and becomes more significant at high temperatures. Ammonia

oxidation can also result in the formation of N<sub>2</sub>O as a byproduct in the absence of NO in the feed, whereas it becomes negligible in the presence of NO<sub>x</sub> and can be removed from the SCR reactions. Furthermore, because NO<sub>2</sub> accounts for only 5% of NO<sub>x</sub>, its reaction can also be ignored in the process.<sup>4</sup>



In this regard, hollow cylindrical catalysts are one of the most commercially viable and applicable catalysts for NH<sub>3</sub>-SCR of NO. The use of catalyst pellets of hollow cylindrical shape provides several distinct advantages over the use of other common shapes and can therefore help to enhance conversion levels in reactors. A better utilization of the catalytic material is probably the most notable of these features because of the absence of a catalyst core, which helps to significantly lower the effect of internal transport resistance. However, there are some drawbacks associated with this type of catalyst. One serious problem that is inherent in the use of hollow cylindrical catalysts, which is similar to that in other types of catalysts with rather wide channels, for example honeycomb catalysts, is that a large proportion of the inlet gas passes through the pore space of the catalyst channel with no serious catalyst engagement and a velocity higher than that of the small fraction that passes through the catalyst layer, which results in lower catalyst utilization and therefore lesser catalytic conversion. Another

Received: May 31, 2014

Revised: July 20, 2014

Accepted: July 22, 2014

Published: July 22, 2014

setback faced by SCR systems is the reactant concentration gradient within the catalyst layer due to resistance of reactant diffusion into the catalyst porous structure, which considerably diminishes the catalyst effectiveness factor.<sup>5</sup> Furthermore, SCR systems face poor activity at low temperatures when most of the NO<sub>x</sub> is produced, e.g., during cold start up and when traveling short distances, which substantially reduces catalyst efficiency and brings about lesser conversion.<sup>6</sup> The chosen method for tackling these setbacks and boosting the De-NO<sub>x</sub> performance of SCR process, especially in terms of hollow cylindrical catalysts, is to make use of an electrohydrodynamic (EHD) technique that is applicable for most mobile and stationary applications and is explicated thoroughly in this study.

So far, this technique has been extensively used as a powerful means of enhancing heat transfer in several investigations. EHD enhancement of heat transfer refers to an interdisciplinary phenomenon dealing with interaction among electric, flow, and temperature fields and can easily be used by applying low-consumption high-voltage electrodes that induce an electrostatic force on a convective flow by polarizing a dielectric fluid under an electrostatic field. Here, some typical examples of EHD technique employment in different applications are presented to show the extent to which this technique is effective and the different ways in which it can be implemented.

Velkoff and Miller first reported the effect of an electric field on condensation heat transfer in 1965.<sup>7</sup> They quoted the increase of mean heat-transfer coefficient by about 200% during condensation of refrigerant R-113 on a flat vertical plate upon the application of an intense electric field perpendicular to a plate. Then, several investigations concerning the EHD-enhanced heat transfer of condensation were carried out by many other researches. For instance, Butrymowicz et al. discussed the mechanism of EHD condensation enhancement and proposed a novel arrangement of a tube–electrode system in their experimental investigations with HCFC-123 as a working medium. Their results indicated that the heat-transfer coefficient increased from 27% to 110%, depending on electrode potential.<sup>8</sup> Sadek et al. also performed an experimental investigation of the EHD augmentation of heat transfer for in-tube condensation of flowing refrigerant HFC-134a in a horizontal heat exchanger with a rod electrode placed in the center of tube. Their experiments showed an enhancement of up to 3.2 times for an 8 kV applied voltage.<sup>9</sup>

Likewise, the enhancing effect of EHD on boiling has been investigated in a number of investigations. Initially, Ogata and Yabe introduced EHD phenomena for promoting bubble generation and augmenting boiling heat transfer. They found an enhancement factor of about 8.5 times that of the maximum value obtained without an electric field.<sup>10</sup> Then, Kweon and Kim performed an experimental investigation of the effect of an electric field on bubble dynamic behavior and the nucleate boiling heat-transfer enhancement of Freon-113 by application of plate–wire electrodes under saturated pool boiling conditions. The results confirmed that the mechanism of EHD nucleate boiling was closely connected with the dynamic behaviors of bubbles and that boiling parameters were significantly changed by the electric field strength and nonuniformity.<sup>11</sup> In addition, P. Wang et al. conducted an experimental study into the influence of a direct current (dc) uniform electric field on the boiling heat-transfer characteristics of liquid nitrogen using a mesh–plane electrode system. Their results showed that electric fields had an obvious effect on

boiling heat transfer of liquid nitrogen.<sup>12</sup> Recently, McGranahan and Robinson investigated the influence of EHD on flow and heat transfer during convective boiling of HFE-7000 in a heat exchanger. Applied voltage across a concentric inner electrode and the outer wall of the tube was varied between 0 and 10 kV at 60 Hz alternating current, and heat-transfer enhancements of up to 1.8-fold were achieved in their experiments.<sup>13</sup>

Furthermore, the application of an electric field has been a promising method for convective heat-transfer enhancement up to the present. Kasayapanand numerically investigated laminar convective heat-transfer enhancement using the EHD technique inside a channel with several electrode arrangements. He also studied the effect of electrode number and electrode arrangement on natural convection.<sup>14–17</sup> Later, Shakouri Pour and Esmaeilzadeh presented an experimental investigation on convective heat-transfer enhancement from three-dimensional heat sources by an EHD actuator in a duct flow.<sup>18</sup> Recently, Baghaei Lakeh et al. investigated natural convection heat-transfer augmentation in circular tubes under the effect of an electric field. They also studied enhancement of convective heat transfer by an electrically induced swirling effect in laminar and fully developed internal flows.<sup>19,20</sup> Deylami et al. also numerically studied the enhancement effect of EHD forces on the amplification of turbulent flow convective heat transfer in a smooth channel using various electrode arrangements.<sup>21</sup> Moreover, Nahavandi and Mehrabani conducted a numerical investigation regarding the EHD effect on natural convection through a vertical enclosure channel for a central processing unit cooling system. Their computational results showed that the heat-transfer coefficient was amplified by more than 1000 kW/cm<sup>2</sup> K with applied voltages up to 100 V.<sup>22</sup>

However, to the best of our knowledge, the effect of EHD on catalytic abatement of pollutants has not been studied. In this study, for the first time, the intensification of selective catalytic reduction of NO by ammonia over vanadia/titania (V<sub>2</sub>O<sub>5</sub>/TiO<sub>2</sub>) catalyst through a hollow cylindrical catalyst has been investigated numerically under the enhancing effect of EHD. This paper first addresses the electrohydrodynamic force and its constitutive derivatives then introduces the EHD-SCR system as well as its proposed model. Next, the defined model without deploying electrode is validated with empirical data from a typical catalytic filter with quasi-cylindrical pores. Finally, simulation results regarding intensified NH<sub>3</sub>-SCR of NO in the EHD-SCR system under different operational conditions are presented and discussed.

## 2. MODELING AND SIMULATION

**2.1. EHD Force.** Electrohydrodynamic force per unit volume is defined as a divergence of the Maxwell electrostatic stress tensor based on eq 3.<sup>22,23</sup>

$$F_i^e = \frac{\partial T_{ij}}{\partial x_j} = E_i \frac{\partial D_j}{\partial x_j} - \frac{\epsilon_0}{2} E_j E_k \frac{\partial \epsilon_{jk}}{\partial x_i} - \frac{1}{2} \frac{\partial}{\partial x_j} (E_i D_j - E_j D_i) \quad (3)$$

In a typical gaseous medium under an electric field, polarization of a dielectric fluid results in energy transfer from free electrons to gas molecules, and the latter move toward the electric field direction. Therefore, distribution of charge density (density of free electrons) and electric field form a Coulomb body force which acts on the charged particles within the fluid and generates a secondary flow that is called

corona wind.<sup>24</sup> This force can be seen in the first term on the right-hand side of eq 3. The second term gives forces at the boundary between two media regions of different dielectric values; the force tends to attract the more polarizable medium into the electric field. The third term is the *i*th component of  $(-1/2) \nabla \times (E \times D)$  and engenders torques and couples in anisotropic media and at surfaces.  $T_{ij}$  and  $D_i$  in this equation are defined in eqs 4 and 5, respectively.<sup>22,23</sup>

$$T_{ij} = \frac{1}{2}(E_i D_j + E_j D_i - E \cdot D \delta_{ij}) = \epsilon_0 \epsilon_r \left( E_i E_j - \frac{1}{2} E^2 \delta_{ij} \right) \quad (4)$$

$$D_i = \epsilon_0 \epsilon_{ij} E_j \quad (5)$$

To define the EHD force for our proposed model described in the next section, eq 4 should be expanded in cylindrical coordinates with its radius and longitudinal components (-*r* and -*z*, respectively) according to eq 6.<sup>22</sup>

$$T_{rz} = \begin{bmatrix} T_{rr} & T_{rz} \\ T_{rz} & T_{zz} \end{bmatrix} \\ = \epsilon_0 \epsilon_r \begin{bmatrix} E_r^2 - \frac{1}{2}(E_r^2 + E_z^2) & E_r E_z \\ E_z E_r & E_z^2 - \frac{1}{2}(E_r^2 + E_z^2) \end{bmatrix} \quad (6)$$

Consequently, the cylindrical derivative of the EHD force can be derived according to eq 7.

$$F^e = \nabla \cdot T = \begin{bmatrix} \frac{1}{r} \frac{\partial}{\partial r}(r T_{rr}) + \frac{\partial}{\partial z} T_{rz} \\ \frac{1}{r} \frac{\partial}{\partial r}(r T_{rz}) + \frac{\partial}{\partial z} T_{zz} \end{bmatrix} \quad (7)$$

**2.2. Model Definition.** To deploy the EHD force in the SCR of NO process, a thin wire electrode can be placed at the center of a hollow cylindrical catalyst (Figure 1). This electrode

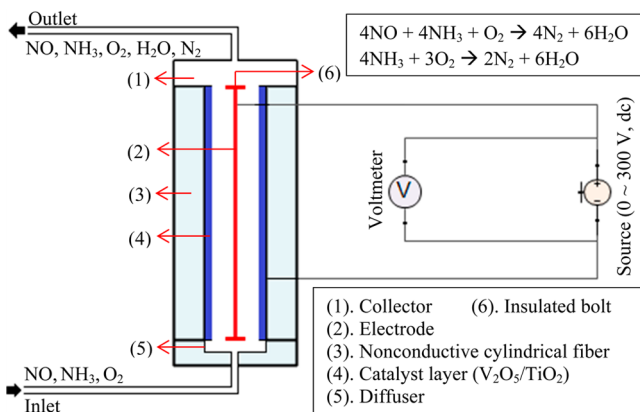


**Figure 1.** Scheme of an electrohydrodynamic selective catalytic reduction (EHD-SCR) system for a hollow cylindrical catalyst.

is fixed from both sides by two electrically insulated bolts and connected to the anode. The entire outer surface of the cylindrical catalyst is covered with a thin metallic sheet and connected to the cathode. In addition, a voltmeter is attached in parallel with the dc source to measure and display the applied electrical voltage. Also, the cylindrical catalyst is surrounded

and held by a nonconductive hollow fiber. As we can see, reacting gases including a high percentage of nitric oxide flow into the catalyst channel from the bottom entrance via a diffuser, and after EHD-intensified SCR reaction over  $V_2O_5/TiO_2$  catalyst, the reacting gases exit from the top of the reactor with a lower percentage of NO, which can be considered as a cleaned gas. This enhanced SCR process that uses EHD as an intensifier is called EHD-SCR method and can be used widely in mobile and stationary applications.

An axial-symmetric system of hollow cylindrical catalyst and its central implemented electrode, which presents a geometrical shape of proposed EHD-SCR system, is shown in Figure 2A. In addition, an orthogonal rectangular field as a longitudinal cross section of the catalyst channel along the fluid flow was taken into consideration for numerical simulation in Figure 2B. Also, Figure 2C presents this rectangular cross section and its interior catalyst layer in a 2D view to show boundary conditions. To see the entire geometry in one domain, as the length of the channel is much longer than its width, the channels length is scaled down  $10^3$  times in this figure. As we can see in Figure 2C, the catalyst layer is placed at the right-hand side beside the catalyst exterior surface with wall with no slip and no mass flux boundary conditions are assumed as the cathode. Also, the anode electrode is placed at the opposite side and is similarly presumed as a wall with no slip and no mass flux boundary conditions. Two other boundaries at the bottom and top of the channel represent input and output of the reacting flow, respectively, with proposed reactant concentrations and gas velocity at inlet and convective concentrations with no viscous stress at outlet under isothermal conditions with no electric charge. The indicated boundary conditions are summarized in Table 1.

The physical and geometrical properties of the hollow cylindrical catalyst modeled in Figure 2 together with operational conditions for numerical simulation are presented in Table 2.

**2.3. Subdomain Equations.** The stationary incompressible Navier–Stokes equation for catalyst free channel and Brinkman equation for catalyst porous medium together with their continuity equations for momentum balance were used in addition to convection–conduction heat-transfer and convection–diffusion mass-transfer equations to describe a steady-state laminar flow of reacting gas through the hollow cylindrical catalyst and were solved simultaneously. These equations are presented in as eqs 8–11.

$$\rho(u \cdot \nabla) u = \nabla \cdot [-pI + \eta(\nabla u + (\nabla u)^T)] + F^e_{\text{catalyst pore space}} \quad (8)$$

$$\left( \frac{\eta}{k_p} + Q \right) u = \nabla \cdot \left[ -pI + \left( \frac{1}{\epsilon_p} \right) \left\{ \eta(\nabla u + (\nabla u)^T) \right. \right. \\ \left. \left. - \left( \frac{2\eta}{3} - k_{dv} \right) (\nabla \cdot u) I \right\} \right] + F^e_{\text{catalyst layer}}$$

$$\nabla \cdot u = \frac{Q}{\rho} \quad (9)$$

$$\nabla \cdot (-k \nabla T) = -\rho C_p u \cdot \nabla T + q \quad (10)$$

$$\nabla \cdot (-D_c \nabla c_i) = -u \cdot \nabla c_i + R \quad (11)$$

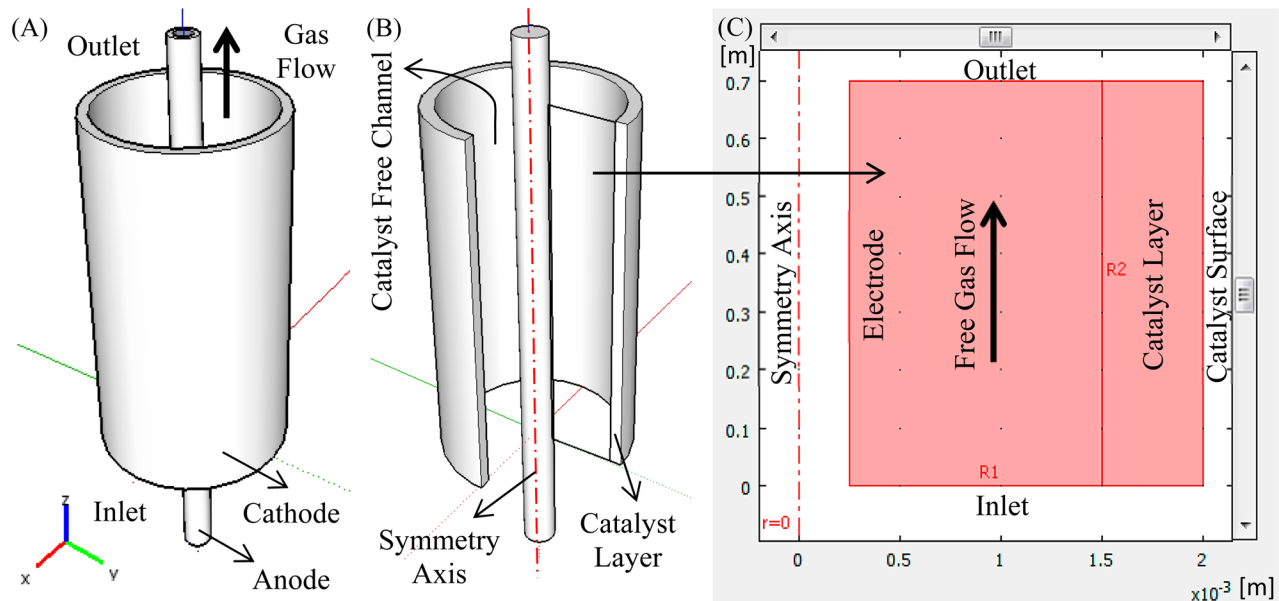


**Figure 2.** EHD-SCR model geometry consists of upward gas flow beside catalyst layer and central electrode: (A) 3D view, (B) 3D view with partly suppressed boundary, and (C) 2D flow field.

**Table 1. Boundary Conditions**

variable	setting			
	inlet <sup>a</sup>	outlet	electrode	catalyst surface
$u$	$2 \times u_{\text{in}} \times (1 - s^2)$	$\eta(\nabla u + (\nabla u)^T)n = 0$	0	0
$c$	$c_j _{\text{in}}$	$n(-D_c \nabla c_j) = 0$	$n(-D_c \nabla c_j + c_j \mu) = 0$	$n(-D_c \nabla c_j + c_j \mu) = 0$
$T$	$T_{\text{in}}$	$n \cdot (-k \nabla T) = 0$	$n \cdot (-k \nabla T) = 0$	$n \cdot (-k \nabla T) = 0$
$V$	$n \cdot D = 0$	$n \cdot D = 0$	$V$	0

<sup>a</sup>The value of  $s$  runs from 0 to 1 along the boundary.

**Table 2. Properties of Hollow Cylindrical Catalyst for EHD-SCR Model Simulation**

Geometry		
catalyst length ( $L$ )	m	0.3–0.7
inside diameter ( $D_{\text{in}}$ )	mm	2.4–3.8
outside diameter ( $D_{\text{out}}$ )	mm	4
catalyst thickness	mm	0.1–0.8
electrode diameter ( $D_e$ )	mm	0.5–1.5
Catalyst Properties		
catalyst	$\text{V}_2\text{O}_5/\text{TiO}_2$ porous homogeneous solid <sup>25</sup>	
$\text{V}_2\text{O}_5$ content	wt %	1–3.45
material porosity	vol %	50
porosity ( $\epsilon_p$ )	vol %	64–82.5
permeability ( $k_p$ )	$\text{m}^2$	$10^{-8}$ <sup>a</sup>
Operating Conditions		
NO inlet concentration	ppm	350
$\text{NH}_3$ inlet concentration	ppm	350
$\text{O}_2$ inlet concentration	vol %	7.6
voltage	V	0–300
temperature ( $T$ )	°C	100–200
GHSV	$\text{h}^{-1}$	10 000–20 000

<sup>a</sup>Extrapolated for  $\epsilon_p = 82.5$  from respective results.<sup>26</sup>

As can be seen from eq 9, the Brinkman equation includes a term that accounts for catalyst permeability and determines the ability of porous medium to allow fluid to pass through it. This coefficient along with fluid pressure drop within the catalyst

medium is strongly dependent on porosity, which overall has a rather negligible effect on catalytic conversion.<sup>26</sup>

Also, the differential form of Gauss's law in the presence of dielectric material that here is considered as a group of gas components was used to define the electrostatic field beside the electrodes according to eq 12.<sup>27</sup> The solution of the electric field forms an EHD force based on eq 7 that was used in momentum balance equations to impose an electric body force on the reacting flow through the cylindrical catalyst space.

$$\nabla \cdot D = -\nabla \cdot \epsilon_0 \epsilon_r \nabla V = \rho_e \quad (12)$$

$$\epsilon_r = \frac{\sum_i C_i \epsilon_{r_i}}{\sum_i C_i}$$

Furthermore, a negligible electric conductivity of the reacting gas which acts as a dielectric material within the catalyst space made it possible for the electric current density to be ignored in the system of equations considered for simulation of the EHD-SCR system.

**3.3.1. Thermodynamic and Transport Properties.** Accurate thermodynamic data is required as input to energy balance equations. The following set of polynomial expressions, eqs 13–15, were used to describe the thermodynamic properties of gas species.<sup>28</sup>

$$C_{p,i} = R_g \sum_{j=1}^5 a_j T^{j-1} \quad (13)$$

$$h_i = R_g \left( \sum_{j=1}^5 \frac{a_j T^j}{j} + a_6 \right) \quad (14)$$

$$S_i = R_g \left( a_1 \ln(T) + \sum_{j=2}^5 \frac{a_j T^{j-1}}{j-1} + a_7 \right) \quad (15)$$

A set of seven coefficients per species are taken as input for the polynomials above for different temperature intervals.<sup>29</sup> The coefficients  $a_1$  through  $a_5$  relate to the species heat capacity; the coefficient  $a_6$  is associated with the species enthalpy of formation (at 0 K), and the coefficient  $a_7$  comes from the species entropy of formation (at 0 K).

In addition to thermodynamic properties, the model equations also require transport properties to accurately describe the space-dependent reactor model. For the reacting gas mixture, transport properties such as binary diffusivities, viscosity, and thermal conductivity were defined as functions of temperature, pressure, and composition using kinetic gas theory. In this regard, the diffusivities and gas viscosity are calculated based on eqs 16 and 17, respectively.<sup>30</sup>

$$D_c = 2.695 \times 10^{-3} \sqrt{\frac{T^3((M_A + M_B)/(2 \times 10^3 M_A M_B))}{\rho \sigma_A \sigma_B \Omega_D}} \quad (16)$$

$$\eta = 2.699 \times 10^{-6} \frac{\sqrt{T(1 \times 10^3 M)}}{\sigma^2 \Omega_V} \quad (17)$$

**2.4. Mesh.** Mapped mesh was used to mesh the 2D cross section shown in Figure 2C in which gas has an upward laminar flow beside the catalyst layer. Because this geometry has a rectangular shape with a length far longer than its width, it can fairly accept mapped elements and simulation can be done more efficiently in comparison with using triangular meshes. As can be seen from Figure 3, rectangular elements with 0.5 mm and 1.25 mm width were applied for catalyst layer and catalyst free channel, respectively. On the other hand, as the solution stability is reduced significantly by application of EHD, especially in this case with a long narrow catalyst space, a

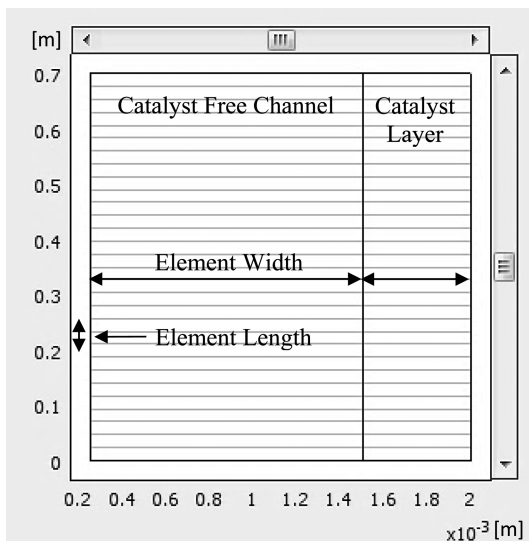


Figure 3. Grid plot; mapped meshes inside 2D cross section.

greater number of elements with smaller lengths must be used in higher electric potentials. Therefore, rectangular elements with a length of 3–7 mm were used for applied voltages between 0 and 300 V to produce a more stable and accurate solution.

**2.4.1. Grid Independence Analysis.** To investigate the independence of the grid from the solution of the problem, the conversion of NO was calculated in different element lengths for various electric potentials and is depicted in Figure 4. As

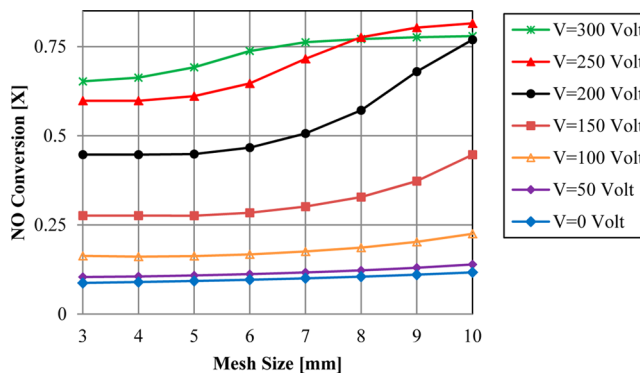


Figure 4. Grid independence analysis; GHSV = 15 000; for other conditions, see Figure 6.

shown, by increasing the mesh size, NO conversion rises moderately because of the lack of accuracy, particularly in higher electric potentials, while it decreases and starts to level off in smaller mesh sizes for different applied voltages, which in turn indicates the independence of the elements from the numerical solution. Table 3 also shows the suitable element lengths based on Figure 4 for different electric potentials.

Table 3. Mapped Mesh Sizes

voltage (V)	0	50	100	150	200	250	300
mesh length (mm)	7	7	6	5	5	4	3

**2.5. Solution Methodology.** In general, modeling an electrohydrodynamic flow is not a trivial task, particularly in an EHD-SCR system as it is described by a system of coupled nonlinear equations consisting of Navier–Stokes and Brinkman equations for reacting flow through catalyst space, Gauss's equation for electric field together with convection–diffusion and convection–conduction equations for mass and heat transfer. Because analytical solutions can be obtained for only a very limited number of cases with the simplest geometry, in the case of such complex systems several techniques and approaches were developed and utilized to arrive at numerical solutions. However, many of them still used some simplifications, such as neglect of diffusion and convection effects in the mass-transport equation, etc. On the other hand, although the governing differential equations of Gauss's law and the EHD force are relatively simple, solving these equations by conventional computational methods does not yield a smooth solution for charge density and electric field. In particular, the results obtained from finite volume method suffer from dispersion errors and fluctuations which lead to distorted values of electric body force and consequently a distorted secondary flow.<sup>24</sup> Therefore, in this study, the finite element method (FEM) was used to solve the system of equations without any simplification. Moreover, Lagrange quadratic

interpolation elements were used to form the finite element interpolation functions. To solve the system of equations, the stationary solver with direct (UMFPACK) module as a linear solution method was used.<sup>31</sup> Also, the relative tolerance and maximum iteration number of  $1 \times 10^{-6}$  and 200, respectively, were set as operational solver parameters for nonlinear setting of the automatic linearity module with damped Newton to solve possible nonlinear system of equations. Furthermore, elimination was chosen for the constraint handling method and no type of scaling was considered for automatic solution form, which was adequate to guarantee the steady solution of the problem.

**2.6. Validation.** To evaluate the validation of simulation data, NO conversion simulated values resulting from NH<sub>3</sub>-SCR over V<sub>2</sub>O<sub>5</sub>/TiO<sub>2</sub> catalyst in the hollow cylindrical catalyst, shown in Figure 2, without a central electrode and the effect of EHD, was compared with empirical results gathered from published experiments for a quasi-pipe passage through a catalytic filter medium. The following reaction rate expressions were considered for kinetic calculation of two indicated parallel reactions in simulation setup (eqs 1 and 2):

$$R_1 = k_1 c_{\text{NO}} \frac{ac_{\text{NH}_3}}{1 + ac_{\text{NH}_3}} \quad (18)$$

$$R_2 = k_2 c_{\text{NH}_3} \quad (19)$$

where,

$$k_j = k_{j0} \exp\left(-\frac{E_j}{R_g T}\right) \quad (20)$$

$$a = a_0 \exp\left(-\frac{A}{R_g T}\right) \quad (21)$$

Selection of these rate equations was inspired by earlier studies regarding intrinsic SCR kinetics.<sup>32,33</sup> The values of constant parameters used in eqs 20 and 21 are presented in Table 4. It should be noticed that few studies concerning the

**Table 4. Parameter Values in Rate Equations**

$E_1 = 60 \text{ kJ/mol}$	$k_{20} = 6.8 \times 10^7 \text{ 1/s}$
$E_2 = 85 \text{ kJ/mol}$	$A = -243 \text{ kJ/mol}$
$k_{10} = 1 \times 10^6 \text{ 1/s}$	$a_0 = 2.68 \times 10^{-17} \text{ m}^3/\text{mol}$

kinetics of ammonia oxidation reaction have been published. However, eq 19 is typically considered for kinetic expression of NH<sub>3</sub> oxidation based on the change of adsorbed ammonia concentration.<sup>34,35</sup> As we can see in Figure 5, NO conversion simulated values agree well with the experimental results with the maximum average deviation of about 1%. Nevertheless, because in this case there is no experimental data to corroborate the simulation results under effect of EHD, any wrong assumption of the model might compromise the obtained results. Here, in particular, it is assumed that the presence of the electric field for the applied voltages between 0 to 300 V does not modify the reaction rate of the SCR process. Also, it is presumed that in this range the transport and thermodynamic properties of the reacting gas are independent of the electric field effects. However, all of these assumptions could not be the case in the presence of high electric field strengths.

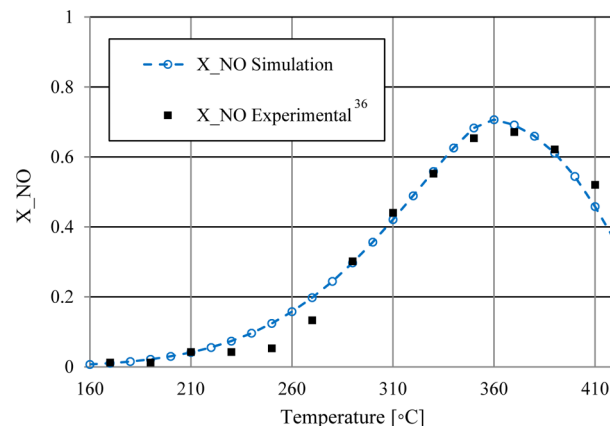


**Figure 5.** Validation of simulation data. Experimental results are from catalytic filter candle experiments using ceramic material in a bench-scale test facility (extracted from published curves:  $y_{\text{NO,in}} = y_{\text{NH}_3,\text{in}} = 350 \text{ ppm}$ ;  $y_{\text{O}_2,\text{in}} = 7.6 \text{ vol \%}$ ; GHSV=11 000).<sup>36</sup>

**2.7. Simulation Results.** The set of steady-state governing equations for our proposed EHD-SCR system was solved using Comsol Multiphysics. According to simulation results, application of EHD technique in catalytic reaction in the form of EHD-SCR system led to a noticeable augmentation of SCR process, despite deficient operational conditions such as low temperature, etc. As can be seen in the following, this system benefited from greater utilization of the catalyst layer, which is reflected in higher NO conversion in addition to its ability to work controllably with an external source of electrical energy.

However, in terms of practical purposes, it should be noted that all of the figures presented here provide numerical data obtained from the simulation of the proposed EHD-SCR system with the specific operational conditions to provide a scientific overview of the EHD-intensified SCR process which might not be practically feasible in many operational applications.

**2.7.1. EHD Enhancement Mechanism.** Mechanism of EHD enhancing effect on catalytic conversion strongly relies on producing internal interaction within the flow field. This interaction causes flow stream lines to veer off its main path in different directions and so makes subordinate movements known as electrohydrodynamically induced secondary flow. In fact, this subsidiary flow is formed as a result of an EHD force induced by applied electrostatic field. As indicated in the EHD Force section, one of the most effective parts of the EHD force expression is Coulomb force. However, because in this case the reacting gas is a neutral fluid without charged ions, this force acts on free electron charges and contorts the electron cloud of gas molecules, which results in induced polarization. The polarized molecules of gas with deformed electron cloud are dragged toward the positive electrode with higher electric field strength. This induced gas flow along with its other incidental movements forms the EHD-induced secondary flow within catalyst space. Here, the variation of the EHD force and its consequent effects on velocity field through catalyst space are first studied to ascertain how the secondary flow leads to more catalytic conversion.

According to panels A.1 and B.1 in Figure 6, electric potential and its consequent EHD force vary between two electrodes within the cylindrical catalyst. As shown in Figure 6A.2, electric potential decreases with distance from anode at different

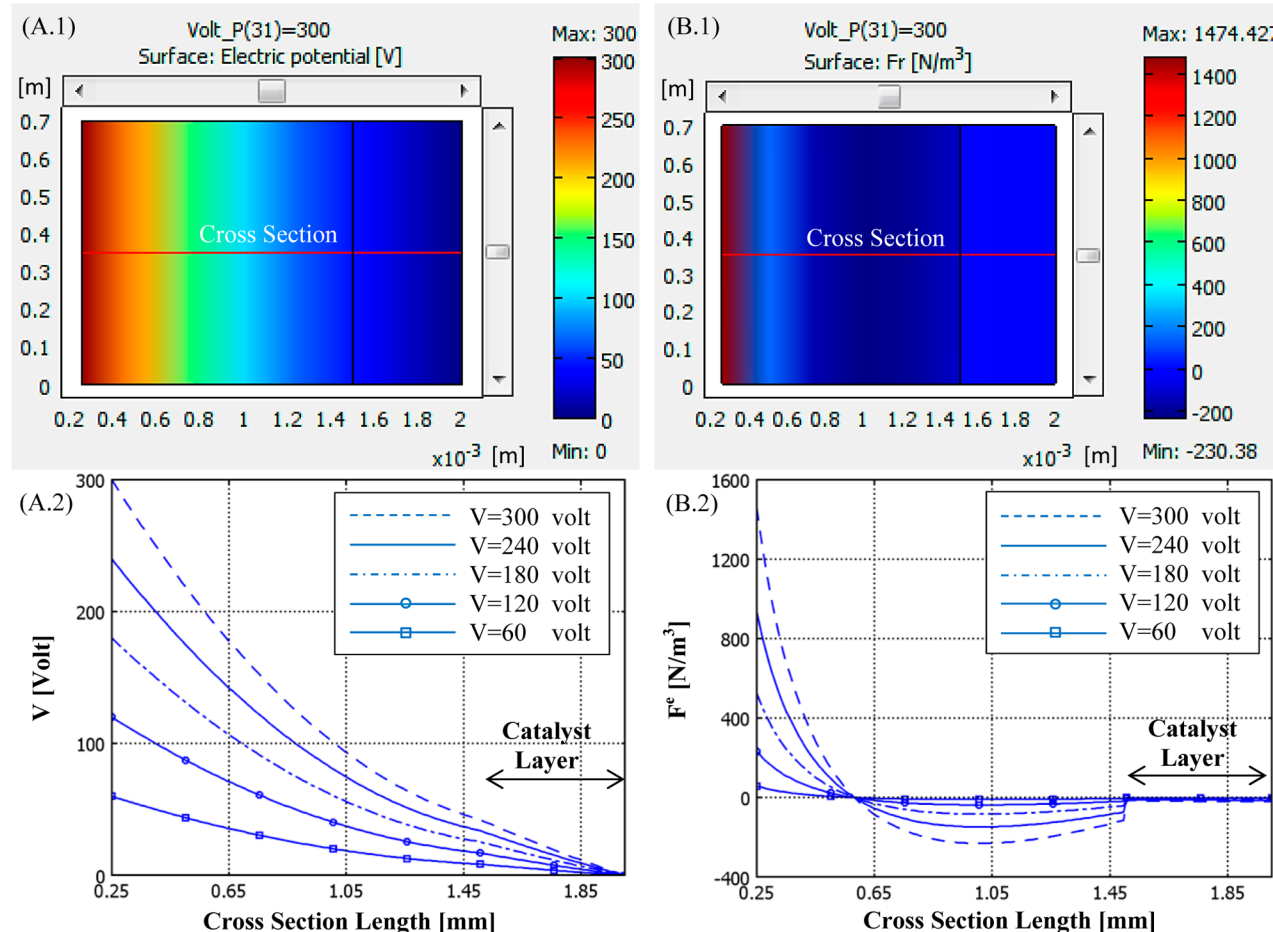


**Figure 6.** Mechanism of EHD enhancing effect; variation of electric potential ( $V$ ) and EHD force ( $F_e$ ) within catalyst space and along cross section in different applied voltages.  $D_e = 0.5$  mm;  $D_{in} = 3$  mm;  $D_{out} = 4$  mm;  $L = 0.7$  m;  $T = 150$  °C; GHSV = 10 000; for other conditions, see Table 2.

applied voltages. This decrease causes considerable decline in the EHD force that primarily acts on free gas flow. As we can see in Figure 6B.2, the downward trend in all applied voltages falls sharply to zero around 0.35 mm from anode surface (known as Debye length or Debye radius), and its falling trend appears to have slowed to reach a minimum value at 1.05 mm. Then, the EHD force rises only slightly and levels off at about zero at 1.5 mm, indicating the beginning of a catalyst layer. The reason why the EHD force within the catalyst layer is almost zero is behind the fact that the more compact a dielectric space is the less the electric potential varies across it, which results in a poorer electric field as a gradient of electric potential and therefore a weaker EHD force as an indirect divergence of the electric field.<sup>23,27</sup> On the other hand, Debye length and its consequent positive EHD force can be referred to as Debye shielding when a cloud of electrons is attracted around the positive surface of anode because of the Coulomb law and balances its positive charge. This great density of negative induced charges forms a shield for the other gas electrons. Therefore, the Debye length is also known as shielding distance because it represents the distance over which the charged surface is shielded from the bulk and the EHD force has a positive value. In contrast, the neighboring gas molecules are dragged by the Coulomb force toward the anode that brings about a negative value for the EHD force, but with a considerably lower strength than that in the Debye region.<sup>37,38</sup> As shown in Figure 6B.2, a less negative value of EHD force is

induced by applying more electric potential, which leads to further drag flow toward the central electrode (anode). This induced effect can be seen more obviously in the deviation of the velocity field. Therefore, variation of radius ( $r$ ) and longitudinal ( $z$ ) components of flow velocity field and their corresponding plots across catalyst space in different applied voltages were investigated and are presented in Figure 7 to show how velocity field is affected by EHD application.

As we can see in Figure 7A.4, by increasing the applied voltage, smaller negative values are achieved for  $V-r$  of gas free flow in the catalyst free channel because of stronger drag force generated by lower negative values of the EHD force shown in Figure 6B.2, which implies more inclination of free flow toward the anode. This induced deflection provides some sort of resistance in the way of upward free flow that leads to gas deceleration within catalyst free channel, Figure 7B.4. Because the primary inward flow has constant velocity, the decelerated flow in the catalyst free channel is compensated by another flow deflection, this time toward the catalyst layer, which is known as the EHD-induced secondary flow. This secondary flow indicates radius deflection of gas into catalyst deeper layers and can be seen from Figure 7A.4 in which  $V-r$  has a positive value in the catalyst layer. Also, according to Figure 7B.4, by raising the applied voltage up to 180 V,  $V-z$  decreases in shallow layers of catalyst medium, which indicates superficial deceleration preceded by full penetration of flow into catalyst layers. As we can see in the following, this penetration reduced

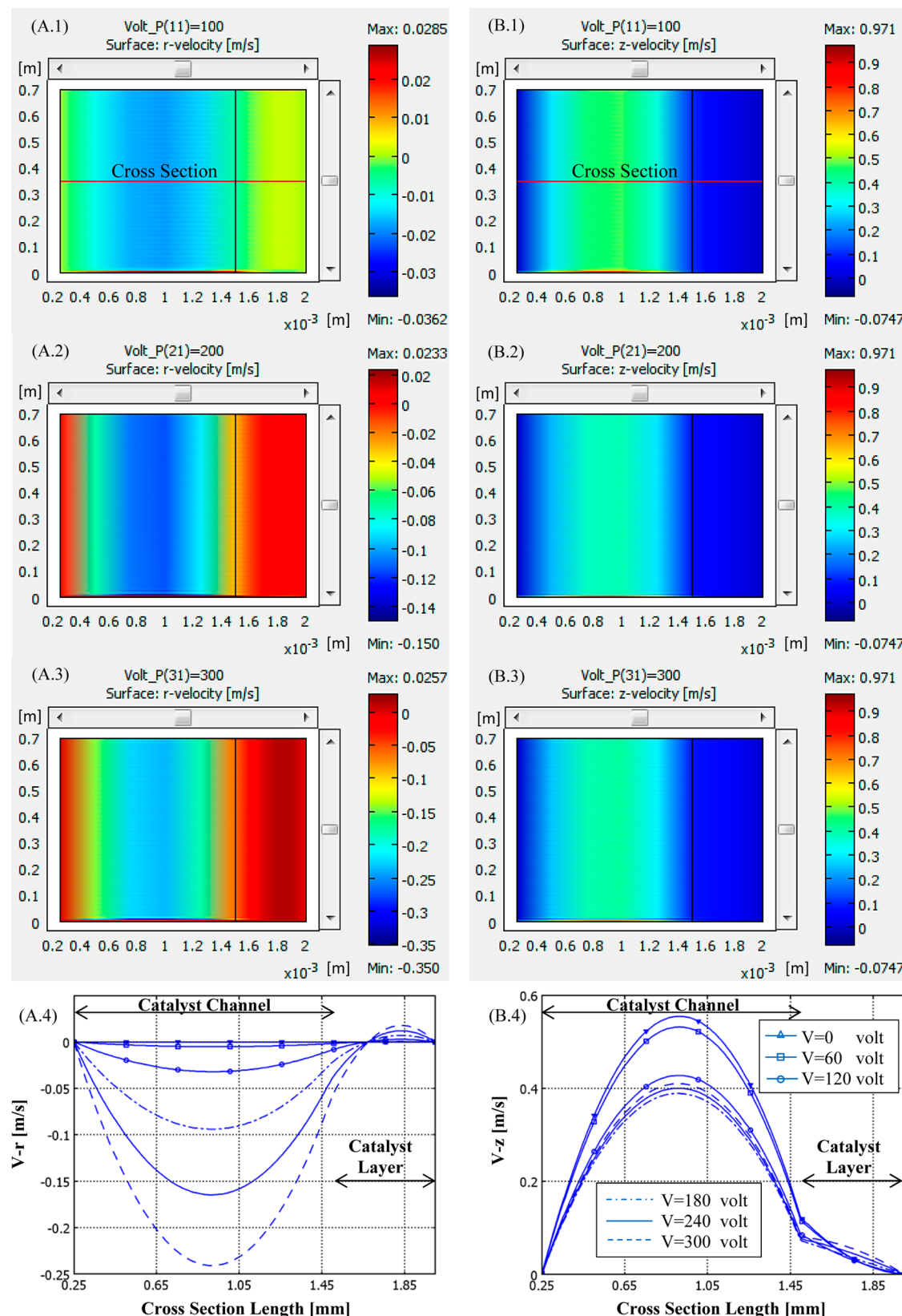


**Figure 7.** Mechanism of EHD enhancing effect; variation of radius and longitudinal components of velocity field ( $V_r$  and  $V_z$ ) within catalyst space and along cross section in different applied voltages; for conditions, see Figure 6.

the diffusion gradient within the catalyst layer. However, although increasing the applied voltage raises the compensatory secondary flow toward deeper layers of the porous medium and

reduces  $V_z$  in the catalyst layer and free channel, as seen in Figure 7B.4, it is no longer the case with the same pattern for applied voltages more than 180 V, when the secondary flow

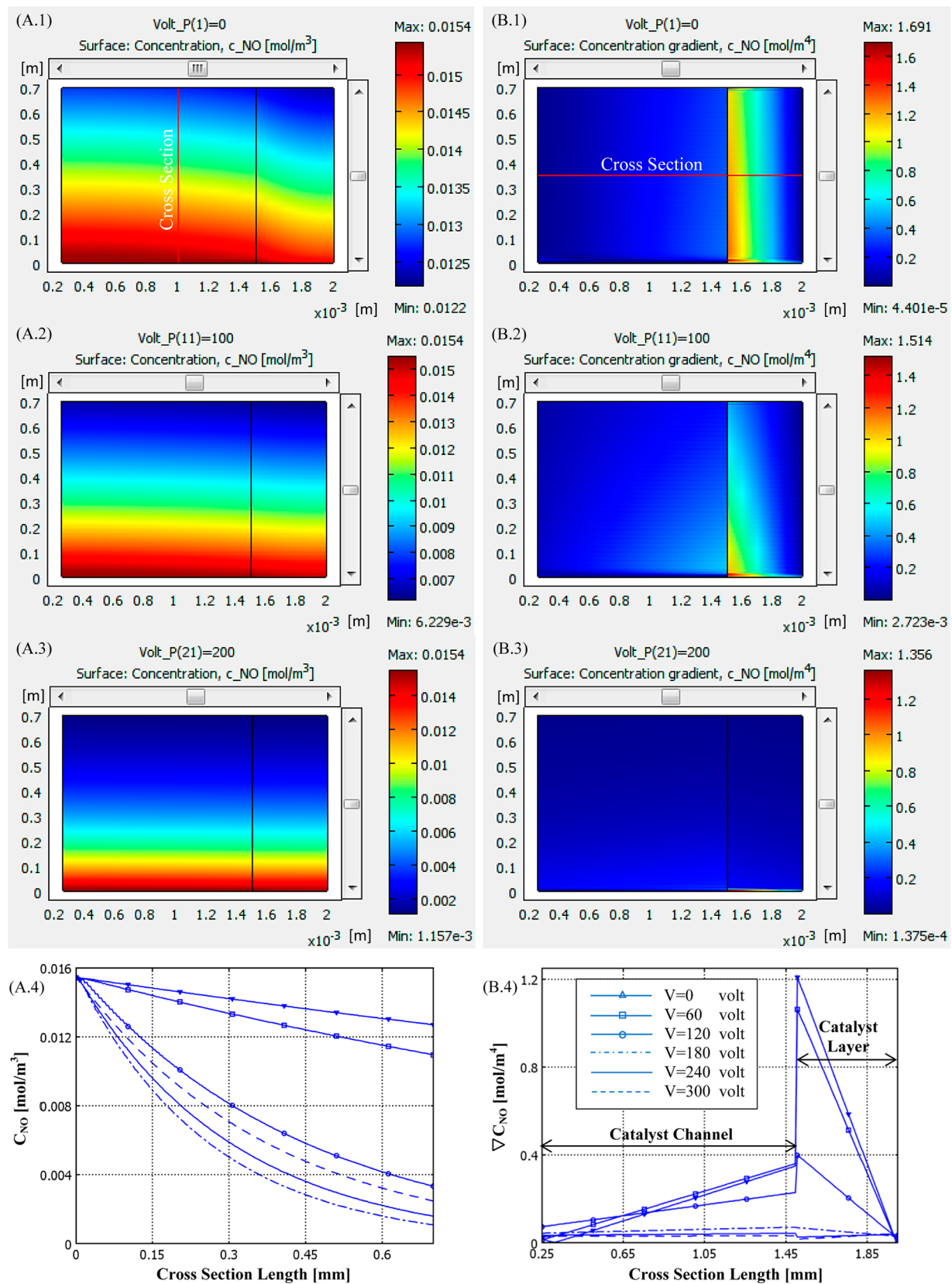


**Figure 8.** Mechanism of EHD enhancing effect; variation of NO concentration and its gradient ( $C_{NO}$  and  $\nabla C_{NO}$ , respectively) through catalyst space and along cross section in different applied voltages; for conditions, see Figure 6.

through the catalyst layer accelerates after full distribution of flow is achieved across the catalyst layer. In addition, because the accelerated reacting flow through the porous structure of

the catalyst layer faces great diffusion resistance, the free flow through the catalyst free channel is pushed ahead by constant momentum of the inward gas stream, which brings about

acceleration in the free flow for applied voltages more than 180 V, Figure 7B.4. Therefore, residence time decreases moderately because of acceleration of reacting gas flow in the catalyst free channel and through catalyst porous layer in particular, which engenders decline in SCR of NO, as described in the following section.

Therefore, one can divide the influence of the EHD force on gas flow through the catalyst space into two positive and negative effects. The former is achieved in moderate electric potentials (here, up to 180 V) and results in flow deceleration followed by increase of residence time and therefore more catalytic conversion, whereas the latter is achieved in higher voltages (here, more than 180 V) with rather opposite implications.

Hence, regardless of the slight negative effects associated with applied voltages higher than 180 V, it is demonstrated that inlet flow deflected to a large extent into the catalyst layer as an EHD-induced secondary flow, while without it a large proportion of gas passes out of the catalyst channel with little catalyst engagement and therefore low catalytic conversion. Thus, catalyst utilization generally increases by application of the EHD technique.

As mentioned, another drawback faced by the SCR system owing to deficient catalyst usage is nonuniform diffusion of the reacting flow into the porous structure of the catalyst layer. In principle, for effective utilization of expensive catalysts, the active material is mostly dispersed on permeable porous supports with large surface area. The reaction takes place at the active catalyst sites, and the product diffuses out. However, the transport of reactant inside the porous network of the catalyst layer is accompanied by diffusion phenomena. Because of transport resistance, reactant concentration in the interior of the catalyst layer is lower than that in bulk free fluid. The consequence of concentration gradients is that reactions occur at different rates depending on the position of the catalyst site within the porous support, which results in a considerable decline in the overall effectiveness of the catalyst.

It is also anticipated here that the EHD force acts in such a way that concentration gradients in the catalyst layer dwindle as a result of uniform gas flow induced through the catalyst porous layer. As indicated earlier, inward gas flow with a high concentration of reactants is funneled into deeper catalyst layers as an EHD-induced secondary flow. Therefore, the mass transport effects in parallel with a concentration gradient are minimized; the overall efficiency of the cylindrical catalyst thereby increases, which results in higher NO conversion, the primary purpose of our EDH-SCR system.

Variation of NO concentration and its gradient through catalyst space and also along proposed cross sections are shown in Figure 8. As can be seen from Figure 8A.4, when the applied voltage is increased to 180 V, NO concentration falls more steeply along the catalyst channel from inlet to outlet. In addition, according to Figure 8B.4, the slope of the NO concentration gradient decreases remarkably across the catalyst channel and particularly across the catalyst porous layer. In contrast, applying voltages higher than 180 V has a rather opposite effect in concentration so that a greater concentration of NO is obtained because of decrease in residence time arising from moderate flow acceleration. However, this does not have notable effect on the concentration gradient because it faces fully uniform flow for electric potentials greater than 180 V. Therefore, as indicated, concentration gradients and therefore mass-transport effects over the catalyst porous layer are reduced

substantially using application of EHD. In the following, we can see how NO conversion for two typical gas flow rates varies at different electric potentials and operating temperatures.

**2.7.2. Effect of Temperature.** As mentioned earlier, poor activity at low temperature is one of the major problems facing SCR systems. It was also demonstrated that application of the EHD technique resulted in better utilization of the catalyst porous layer as a passive catalytic potential can significantly ameliorate catalyst effectiveness as well as its conversion performance. This is even more important, particularly in terms of NO reduction, because the reduction is a primary objective of the operation of the SCR system. It is therefore crucial to identify the extent to which EHD application is effective at different temperatures and to what degree this technique can compensate the negative effect of low temperatures in different applied voltages, which is so decisive in selection of the most effective operational conditions. To this end, variation of NO conversion and its enhancement versus electric potential at different operating temperatures was investigated; the results are shown in Figure 9. As we can see in Figure 9A, NO

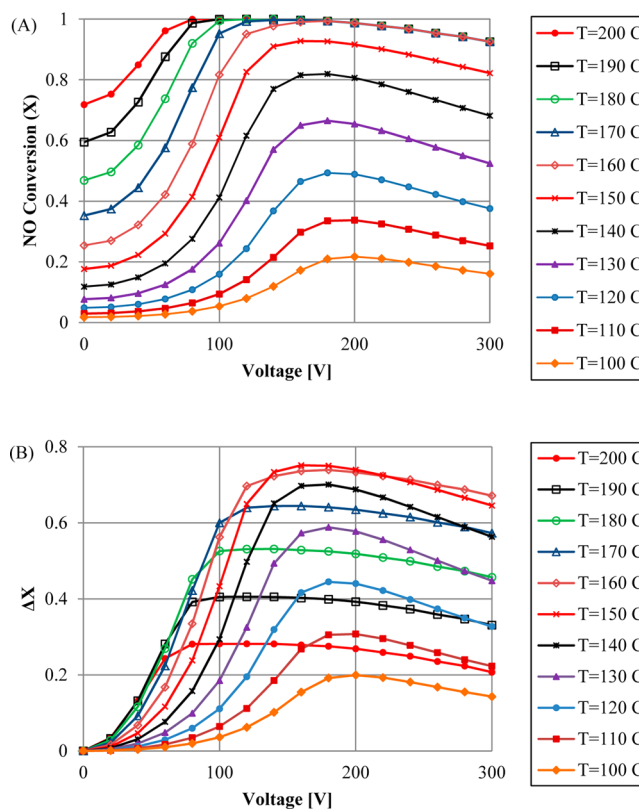


**Figure 9.** Effect of temperature on NO conversion (A) and NO conversion enhancement (B) versus applied voltage.  $\Delta X = X_v - X_{v=0}$ ; GHSV = 10 000; for other conditions, see Figure 6.

conversion increases remarkably by raising the applied voltage up to almost 180 V for operating temperatures up to 150 °C. Then NO conversion begins to fall for higher applied voltages because of lower residence time of the reacting flow resulting from flow acceleration through the catalyst layer, as explicated earlier. Also, by raising the temperature above 150 °C, NO conversion soars to 1 but in voltages lower than 160 V and then again starts to decline from 180 V as before. To show the extent to which NO conversion is enhanced using the EHD technique at different operating temperatures and electric potentials, NO

conversion enhancement in the form of conversion differences was also studied; the results are displayed in Figure 9B. As seen, for temperatures less than 160 °C, all curves peak in applied voltages between 160 and 200 V; the maximum of about 0.75 is achieved in 160 V for 150 °C. In contrast, other curves with higher operating temperatures peak in lower applied voltages and with moderate downward trends for higher electric potentials.

Similar trends also were achieved for GHSV of 15 000, which can be seen in Figure 10. In comparison with Figure 9, NO

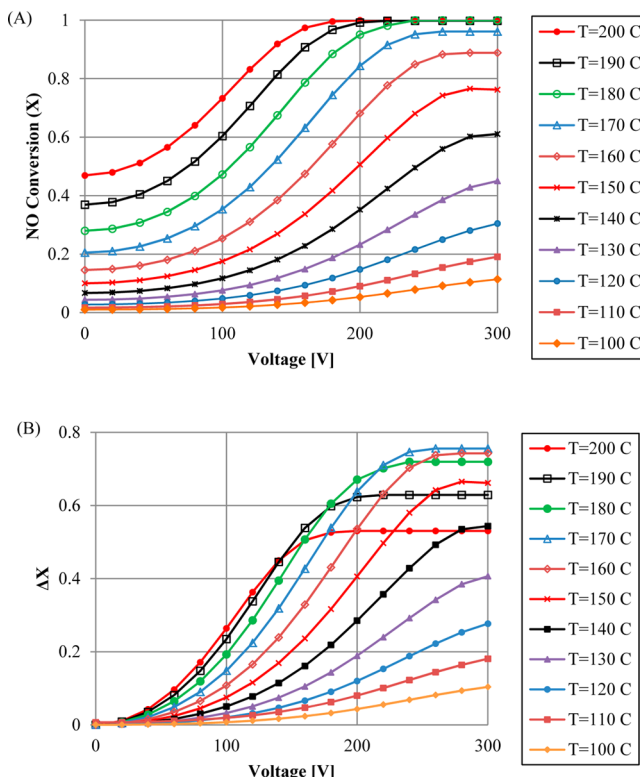


**Figure 10.** Effect of temperature on NO conversion (A) and NO conversion enhancement (B) versus applied voltage.  $\Delta X = X_v - X_{v=0}$ ; GHSV = 15 000; for other conditions, see Figure 6.

conversion as well as its growing differences peak in higher applied voltages with lower values than those which were obtained for GHSV of 10 000. For example, at typical operating temperature of 150 °C, both trends shown in panels A and B of Figure 10 peak at about 0.76 and 0.66, respectively, in 300 V, compared to 0.92 and 0.75 in just 180 V for GHSV of 10 000 shown in Figure 9. In the following, the effect of gas velocity and its subsequent results are explained in greater detail. Nonetheless, as demonstrated, NO conversion even at low operating temperatures and therefore low catalyst activities increases substantially by application of EHD in certain electric potentials, although the higher conversions are achieved at greater temperatures. Thus, because catalytic conversion is to a large extent under the effect of temperature, NO conversion and its enhancement versus operating temperature were investigated in different applied voltages, which led to further noticeable results and patterns.

As can be seen from Figure 11A, when the temperature increases, conversion rises more steeply in higher applied voltages. As the voltage approaches around 180 V, NO conversion faces lesser changes and is more overlaid with

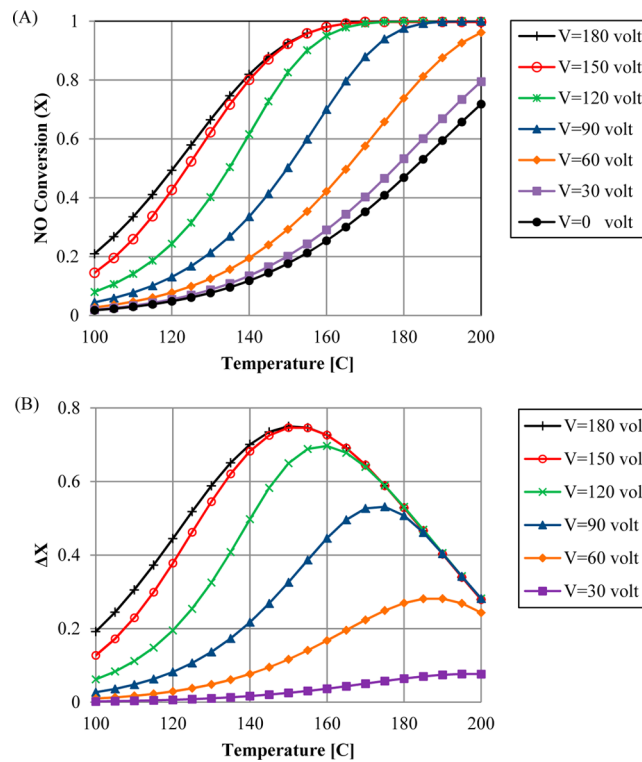


**Figure 11.** Effect of applied voltage on NO conversion (A) and NO conversion enhancement (B) versus operating temperature.  $\Delta X = X_v - X_{v=0}$ ; GHSV = 10 000; for other conditions, see Figure 6.

nearby trends. Figure 11B also illustrates NO conversion enhancement in the form of conversion differences and presents the operating temperatures at which the conversion has its maximum EHD enhancement in different applied voltages. As we can see, the figure peaks at close to 0.75 in 150 °C for applied voltage of 150 V with little variance from that of 180 V, which implies the condition of almost maximum enhancement, although the exact maximum point was obtained at 160 V according to Figure 9B. In fact, on the basis of Figure 11B, when electric potential is increased, the conversion enhancement reaches its maximum with upper values in lower temperatures, while in higher temperatures, enhancement curves overlap each other much further. Eventually, by approaching 180 V, no considerable change occurs in the maximum value, which can be considered as the maximum enhancement with the most overlap and least possible temperature.

There are also similar trends concerning higher gas velocities, which can be seen in Figure 12 for GHSV of 15 000. Figure 12A shows that NO conversion increases most steeply in 270 V by raising operating temperature. Also, on the basis of Figure 12B, the maximum conversion enhancement is obtained at about 0.75 in 165 °C and 270 V compared to the almost similar maximum value in 150 °C and just 150 V for GHSV of 10 000 shown in Figure 11B. Although the value of maximum enhancement hasn't changed by increasing gas velocity, it has been achieved in notably lower voltage and also rather lower temperature, which therefore indicates the prominent influence of gas flow velocity on EHD enhancement of NO conversion.

**2.7.3. Effect of GHSV.** As indicated, NO conversion is substantially under the effect of gas velocity, so that it declines at higher gas velocities with the same operational conditions. Actually, this effect refers to alterations in residence time. When

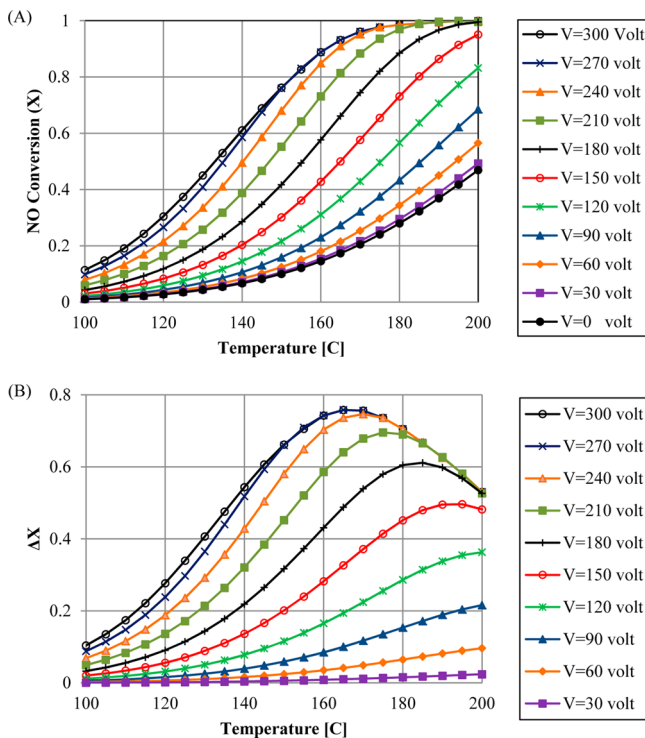


**Figure 12.** Effect of applied voltage on NO conversion (A) and NO conversion enhancement (B) versus operating temperature.  $\Delta X = X_v - X_{v=0}$ ; GHSV = 15 000; for other conditions, see Figure 6.

gas velocity in a constant electric potential is increased, the momentum of the upward gas stream dominates the movement resistance associated with decelerated flow of the catalyst free channel. Therefore, residence time of the reacting gas through catalyst space and particularly within the catalyst layer decreases as a result of gas flow acceleration, which brings about lower NO conversion. However, although conversion decreases moderately at high electric potentials because of this effect, because of the greater movement resistance induced in higher applied voltages, conversion is less affected by increasing gas velocity. For more clarification, a typical comparison was made in Figure 13 to investigate the undermining effect of greater gas velocity on catalytic conversion. As we can see, for GHSV of 10 000, NO conversion peaks significantly at close to 0.92 when the applied voltage increases to 150 V, whereas it experiences a great drop by shifting to 15 000 GHSV. Then, conversion starts

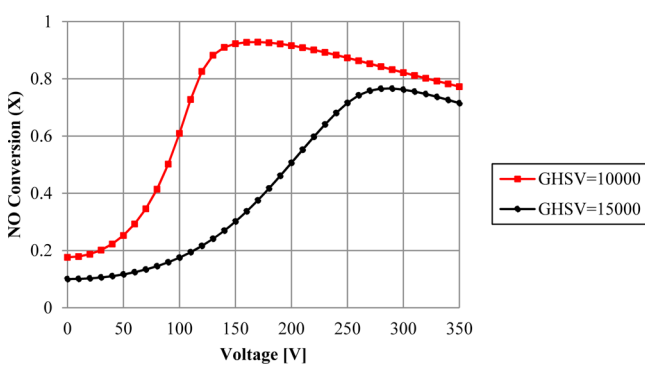


**Figure 13.** Effect of GHSV on NO conversion versus applied voltage: comparison between two typical gas velocities. For conditions, see Figure 6.

to decrease moderately from 180 V, whereas for GHSV of 15 000, conversion proceeds to climb up to almost 0.76 at 300 V and begins falling after that by a trend parallel to that of GHSV of 10 000. Therefore, as explained, decreasing effect of increasing gas velocity tends to be minimized for applied voltages higher than 300 V.

In addition, to study the effect of gas flow velocity more precisely in different applied voltages, variation of NO conversion and its enhancement versus GHSV are presented in Figure 14. As can be seen from Figure 14A, when GHSV is

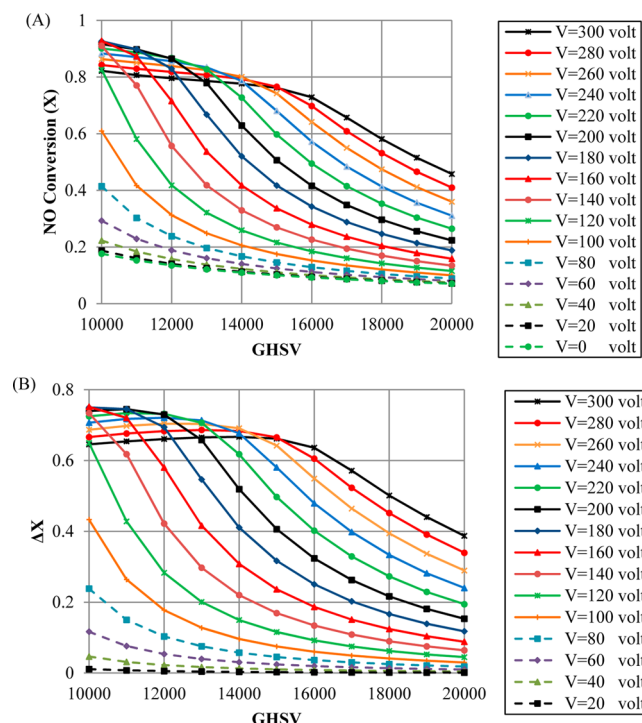


**Figure 14.** Effect of GHSV on NO conversion (A) and NO conversion enhancement (B) in different applied voltages.  $\Delta X = X_v - X_{v=0}$ . For conditions, see Figure 6.

increased, NO conversion decreases substantially for electric potentials up to 180 V while it decreases more steadily for higher applied voltages especially at lower gas velocities. Also, according to Figure 14B, there are maximums with lower values in higher GHSV for electric potentials greater than 180 V that specify gas velocities in which maximum enhancements are obtained for respective applied voltages.

Therefore, generally higher EHD enhancement of NO conversion is achieved in lower GHSVs, which can also be seen for the thermal enhancing effect of EHD that is dominant in low gas velocities.<sup>24</sup>

**2.7.4. Effect of Catalyst Layer Thickness.** The catalyst porous layer is the most operational part of the SCR system, where the entire chemical reactions take place. Therefore, its geometrical size, especially its thickness, substantially influences catalytic conversion. It is sensible that by penetration of the reacting flow into a wider catalyst layer, a larger active area of the porous medium becomes available for the proposed chemical reactions and a higher conversion is achieved. Because applying an electric potential results in the reacting flow tending to penetrate further into the catalyst layer in the form of EHD-induced secondary flow, a wider catalyst layer provides additional gas penetration. Therefore, reactant conversion

increases more steeply by increasing the applied voltage in thicker catalyst layers. However, by increasing gas penetration into a wider catalyst layer, uniform flow through the catalyst porous medium is obtained at lower electric potentials where applying higher voltages leads to moderate decrease in residence time and therefore catalytic conversion. As shown in Figure 15A, NO conversion increases more steeply by raising

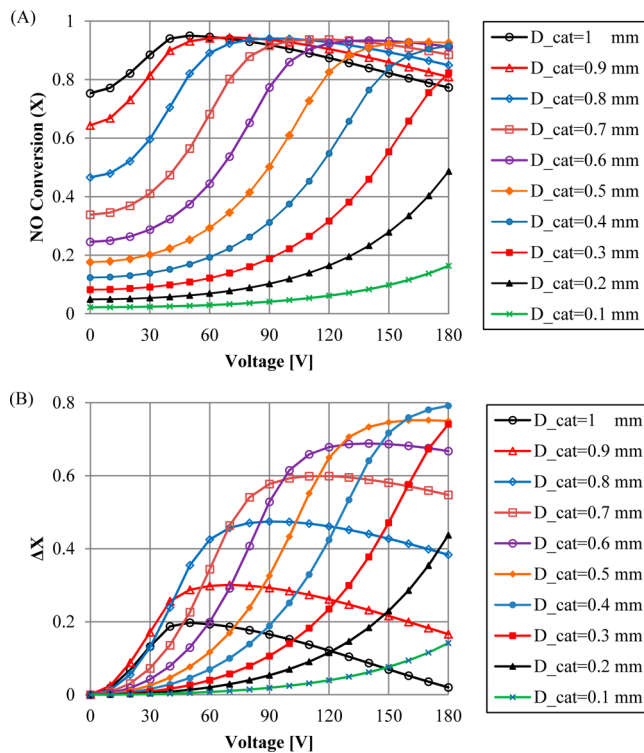


**Figure 15.** Effect of catalyst layer thickness on NO conversion (A) and NO conversion enhancement (B) versus applied voltage. For conditions, see Figure 6.

applied voltage in thicker catalyst layers. It can also be seen that by application of wider catalyst layers, NO conversion starts to decline in lower voltages for higher electric potentials. In addition, regardless of the catalyst layer thickness, the maximum conversion of about 0.93 is achieved for all curves in certain applied voltages. Furthermore, Figure 15B illustrates NO conversion enhancement for various catalyst layers and electric potentials. As seen, by increasing the applied voltage, EHD enhancement in the form of conversion differences climbs more steeply to reach a peak of about 0.80 at 180 V for a 0.4 mm catalyst layer. Also, according to this figure, there are some maximums in the conversion enhancement for catalyst layers wider than 0.5 mm with lesser values in lower electric potentials (Figure 15A), which indicate negative effect of flow acceleration mainly after reaching uniform flow pattern within the catalyst layer as explained before. In the next section, we describe how electrode diameter influences EHD-intensified conversion of NO and its enhancement level.

**2.7.5. Effect of Electrode Diameter.** Influence of electrode diameter on catalytic conversion is rather similar to catalyst layer thickness as the catalyst channel becomes narrower, but with an obvious difference. In this case, when the electrode diameter is increased at the constant thickness of catalyst layer, chemical reactions take place in a specified volume of the catalyst layer medium with given active sites. Hence, it is

anticipated that NO conversion does not increase as much as that seen previously for thicker catalyst layers. However, by implementing thicker electrodes, a thinner catalyst free channel is provided for free flow, and as a result, the reacting gas funnels more into the catalyst layer to make more utilization of the catalyst layer and diminish the negative effect of diffusion gradient. As explained before, more penetration of the reacting gas in the form of EHD-induced secondary flow provides more uniform flow through the catalyst layer, which results in greater catalytic conversions. However, this EHD positive effect can be undermined by decreasing residence time because of flow acceleration resulting from high electric potentials, particularly in the presence of wide anodes, which inflicts lower conversion on the EHD-SCR system in the way of reaching fully uniform flow in the catalyst layer with the maximum effectiveness.

As we can see in Figure 16A, NO conversion increases more steeply by increasing the applied voltage in the presence of

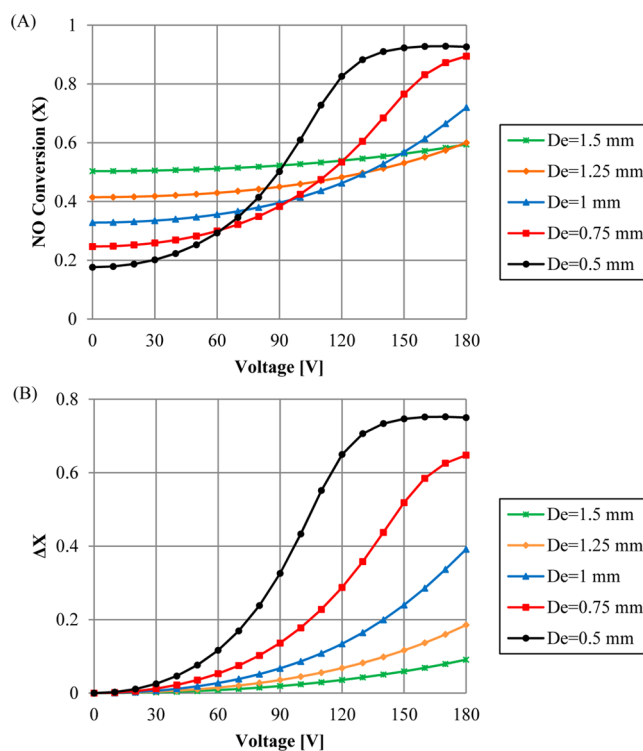


**Figure 16.** Effect of electrode diameter on NO conversion (A) and NO conversion enhancement (B) versus applied voltage. For conditions, see Figure 6.

thinner electrodes. As shown, NO conversion peaks at close to 0.93 in the presence of 0.5 mm electrode diameter in 180 V. On the other hand, although NO conversion has higher values in the presence of thicker electrodes for low applied voltages, increasing electric potential has less influence on conversion enhancement because of the undermining effect of flow acceleration. Therefore, as shown in Figure 16A, no significant increase can be gained for electrode diameter of 1.5 mm. In fact, when higher voltages are applied, the enhancing effect of fluid penetration into deeper catalyst layers in the form of EHD-induced secondary flow is neutralized by the negative effect of fluid acceleration that is more significant in the presence of thicker electrodes.

Furthermore, noticeable trends regarding enhancement of NO conversion in the form of conversion differences versus electric potential were obtained and are presented in Figure 16B. According to this figure, NO conversion enhancement rises more steeply by raising applied voltage in thinner electrodes so that the maximum increase of almost 0.75 is achieved for NO conversion by implementing a 0.5 mm electrode diameter in 180 V.

**2.7.6. Effect of Catalyst Length.** As mentioned earlier, more conversions are achieved when chemical reactions take place within a wider catalyst layer with more available active sites in the porous medium. However, the same is not always true when it comes to the catalyst length, as the major fraction of total conversion is obtained through the beginning of the catalyst with higher concentration gradient. Hence, the remaining catalyst length away from the catalyst entrance is left less effective and increasing the length of the catalyst makes a slight contribution to overall conversion. However, as EHD application causes reacting gas flow to funnel further into catalyst layer in the form of EHD-induced secondary flow, catalyst length becomes more effective in moderate electric potentials; it remains almost ineffective in higher applied voltages because of negative effect of flow acceleration. Therefore, as can be seen from Figure 17, NO conversion varies only slightly in low and high electric potentials for different catalyst lengths.

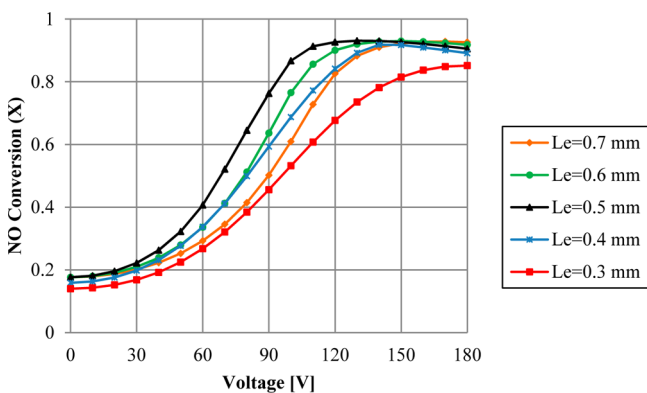


Figure 17. Effect of catalyst length on NO conversion versus applied voltage. For conditions, see Figure 6.

**2.7.7. Electrical Energy.** Energy consumption is one of the most controversial issues of any operational system dealing with using some sort of power or energy. There is an outstanding similarity between our proposed EHD-SCR system and a typical electric capacitor: in both of them, an electrical insulator, the so-called dielectric material, is placed between two electrodes with opposite electric charges, namely, cathode and anode. The only difference is that here the dielectric material is the reacting gas with a tiny polarizability and therefore a small relative permittivity, known as the dielectric constant, with an average of around 1 in comparison to common dielectrics with higher dielectric constants used in commercial capacitors. Because the components of the gas flow and therefore its average electric permittivity between two electrodes in the EHD-SCR system fluctuate by changing electric potential due to different conversion of reactants especially to water vapor with rather more polarizability, the capacitance of the system as a quasi-capacitor was first calculated according to eq 22.<sup>39</sup> Then, on the basis of the given results, applied energy, which

can be constituted as a stored energy within the common capacitor, was calculated in different electric potentials based on eq 23<sup>39</sup> and is presented in Figure 18.

$$C = \frac{2\pi\epsilon L}{\ln\left(\frac{D_{out}}{D_{in}}\right)} \quad (22)$$

$$W = \frac{1}{2}CV^2 \quad (23)$$

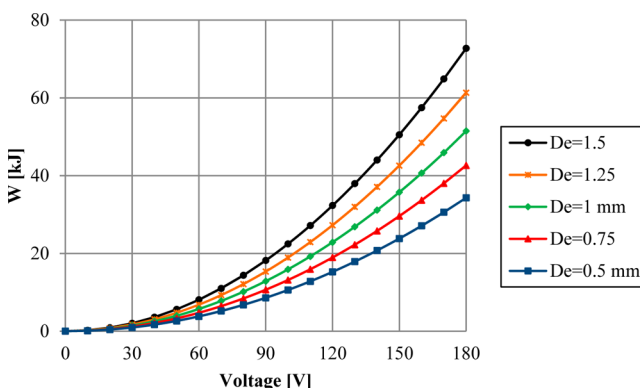


Figure 18. Electrical energy consumption versus applied voltage in different electrode diameters. For conditions, see Figure 6.

As shown, when electric potential increases, applied electrical energy increases more steeply in the presence of a thicker anode as a central electrode, which implies that more energy is consumed in a narrower catalyst free channel with higher electric capacitance in parallel with a stronger electric field followed by a higher EHD force; therefore, there is more catalytic conversion.

In addition, because the electric current density in the gas is very low and the EHD force is substantially dependent on electric field strength as a gradient of electric potential, providing a high-voltage electric source for the EHD-SCR system is inevitable. On the other hand, as the available electrical energy in automobiles can be simply converted into high voltage low amperage electric current (~300 V, dc) using electrical converters, the application of the EHD-SCR system in various types of cars and vehicles is practically feasible in addition to application of the EHD-SCR system in stationary applications.

### 3. CONCLUSIONS

In this work, initially the importance of heterogeneous catalysis in catalytic abatement of NO using NH<sub>3</sub>-SCR over V<sub>2</sub>O<sub>5</sub>/TiO<sub>2</sub> catalyst was illustrated. Next, a hollow cylindrical catalyst together with its operational advantages and disadvantages was introduced. Hence, the EHD technique as a promising method of eliminating those drawbacks was suggested and the EHD-SCR system presumed as a functional model for implementation of this technique. Then, a computational study was conducted under various operational conditions to verify the extent to which this method was effective and examine the effect of different parameters on EHD-enhanced conversion of NO in the proposed model. On the basis of acquired simulation results, NO conversion was intensified significantly by more than 4.2-fold (equivalent to 0.75 increase in NO conversion)

using the EHD-SCR system. In general, the following conclusions can be drawn from this investigation:

- (1) Application of the EHD technique to a large extent managed to eradicate undermining effect of concentration gradient within the catalyst layer by facilitating mass transfer into the catalyst layer via introducing a subsidiary flow known as EHD-induced secondary flow through the catalyst porous medium.
- (2) EHD enhancement of reactant conversion is substantially under the effect of electric potential. However, applying higher voltages does not necessarily favor more NO conversion as flow acceleration through the catalyst layer diminishes catalytic conversion.
- (3) Identification of the most efficient operational conditions in which the maximum enhancement of NO-SCR is achieved strongly depends on operating temperature, so that the maximum performance of the EHD-SCR system was obtained in specific temperatures by applying different electric potentials. As a result, the maximum increase of almost 0.75 was achieved for NO conversion in 150 and 165 °C for applied voltage of 150 and 270 V, respectively.
- (4) In general, increasing the velocity of the gas stream flowing through catalyst space reduces NH<sub>3</sub>-SCR of NO. However, when higher voltages are applied, the negative effect of raising gas velocity declines significantly, although conversion diminishes relatively in higher electric potentials under the undesirable effect of flow acceleration within the catalyst layer.
- (5) Catalyst layer thickness substantially influences EHD-SCR enhancement, so that by increasing applied voltage in a thicker catalyst layer conversion increases more steeply although it has opposite effect in thicknesses more than 0.4 mm. Results showed that the maximum increase of about 0.80 could be achieved for NO conversion in the presence of a 0.4 mm catalyst layer thickness for 180 V and 150 °C.
- (6) According to the obtained results, application of a thicker electrode (anode) in the center of the catalyst channel generally has negative effect on EHD-SCR enhancement, although higher conversions are achieved in lower voltages. As a result, the maximum increase of almost 0.75 was obtained for NO conversion in the presence of 0.5 mm electrode diameter for 180 V and 150 °C compared to just 0.09 for 1.5 mm electrode diameter.
- (7) NO conversion was affected by catalyst length only in moderate electric potentials.
- (8) Electrical energy consumption increased more significantly by increasing applied voltage in the presence of thicker electrodes. On the basis of simulation results, the maximum energy of 72.73 kJ was used for 1.5 mm electrode diameter in 180 V and 150 °C.

## AUTHOR INFORMATION

### Corresponding Author

\*Phone: +98-9183517159. E-mail: m.nahavandi@ce.iut.ac.ir.

### Notes

The authors declare no competing financial interest.

## NOMENCLATURE

$F_i^e$  = Electrohydrodynamic (EHD) Force (N/m<sup>3</sup>)

$T_{ij}$  = Maxwell electrostatic stress tensor (Pa)

- $D$  = Charge displacement (V/m)  
 $\eta$  = Dynamic viscosity (Pa.s)  
 $E$  = Electric field (V/m)  
 $\epsilon_r$  = Relative electric permittivity (C/V·m)  
 $\epsilon_0$  = Electric permittivity of vacuum:  $3.32032 \times 10^{-15}$  (C/V·m) or (F·m)  
 $\delta_{ij}$  = Unit tensor  
 $u$  = Velocity (m/s)  
 $V$  = Electric voltage (V)  
 $g$  = Gravitational acceleration vector (m/s<sup>2</sup>)  
 $k_{dv}$  = Dilatational viscosity (Pa s)  
 $n$  = Normal unit vector  
 $q$  = Heat source (W/m<sup>3</sup>)  
 $\rho$  = Fluid density (kg/m<sup>3</sup>)  
 $k$  = Thermal conductivity (W/m·K)  
 $c_i$  = Concentration (mol/m<sup>3</sup>)  
 $p$  = Pressure (Pa)  
 $k_p$  = Permeability (m<sup>2</sup>)  
 $Q$  = Source term (in Brinkman equation) (kg/(m<sup>3</sup>.s))  
 $\epsilon_p$  = Porosity  
 $C_p$  = Heat capacity at constant pressure (J/(kg.K))  
 $R$  = Reaction rate (mol/(m<sup>3</sup>.s))  
 $I$  = Unit vector  
 $R_g$  = Universal gas constant: 8.31441 (J/(mol. K))  
 $T$  = Temperature (K)  
 $A$  = Frequency factor  
 $E_j$  = Activation energy (J/mol)  
 $k_i$  = Reaction rate constant  
 $X$  = Conversion  
 $D_c$  = Diffusion coefficient (m<sup>2</sup>/s)  
 $C$  = Capacitance (C/V) or (F)  
 $L$  = Catalyst length (m)  
 $W$  = Electrical energy (J)  
 $\rho_e$  = Electric charge density (C/m<sup>3</sup>)  
 $h_i$  = Species' molar enthalpy (J/mol)  
 $s_i$  = Species' molar entropy (J/(mol.K))  
 $C_{pi}$  = Species' heat capacity (J/(mol.K))  
 $\sigma$  = Characteristic length of the Lennard-Jones interaction potential:  $10^{-10}$  (m)  
 $\sigma_A$  = Molecular diameter of A (m)  
 $\sigma_B$  = Molecular diameter of B (m)  
 $\Omega_D$  = Collision integral  
 $\Omega_V$  = Collision integral  
 $M_A$  = Molar weight of A (kg/mol)  
 $M_B$  = Molar weight of B (kg/mol)

## Abbreviations

- SCR = Selective catalytic reduction  
EHD = Electrohydrodynamics  
GHSV = Gas hourly space velocity  
De-NO<sub>x</sub> = NO<sub>x</sub> removal  
UMFPACK = Unsymmetric MultiFrontal method  
dc = Direct current  
ac = Alternating current

## REFERENCES

- (1) Xu, W.; Yu, Y.; Zhang, C.; He, H. Selective catalytic reduction of NO by NH over a Ce/TiO catalyst. *Catal. Commun.* **2008**, *9*, 1453–1457.
- (2) Kobayashi, Y.; Tajima, N.; Nakano, H.; Hirao, K. Selective catalytic reduction of nitric oxide by ammonia: The activation mechanism. *J. Phys. Chem. B* **2004**, *108*, 12264–12266.
- (3) Vega, E. M.; Garcia, S. O.; Sanz, F. V. D'Ammonia selective catalytic reduction of NO in a Monolithic reverse flow reactor.

Proceedings of Icheap-10: Tenth International Conference on Chemical & Process Engineering, Florence, Italy, May 8–11, 2011 1–3.

(4) Nova, I.; Beretta, A.; Groppi, G.; Lietti, L.; Tronconi, E.; Forzatti, P. Monolithic catalysts for NO<sub>x</sub> removal from stationary sources. In *Structured Catalysts and Reactors*; Cybulski, A., Mouljin, J. A., Eds.; CRC Press: Boca Raton, FL, 2006; 171–214.

(5) Asif, M. Conversion in chemical reactors using hollow cylindrical catalyst pellet. *Int. J. Chem. Environ. Eng.* **2012**, *6*, 178–183.

(6) Forzatti, P.; Nova, I.; Tronconi, E. New “Enhanced NH<sub>3</sub>-SCR” Reaction for NO<sub>x</sub> Emission Control. *Ind. Eng. Chem. Res.* **2010**, *49*, 10386–10391.

(7) Velkoff, H. R.; Miller, J. H. Condensation of vapor on a vertical plate with a transverse electrostatic field. *J. Heat Transfer* **1965**, *87*, 197–201.

(8) Butrymowicz, D.; Trella, M.; Karwacki, J. Enhancement of condensation heat transfer by means of EHD condensate drainage. *Int. J. Therm. Sci.* **2002**, *41*, 646–657.

(9) Sadek, H.; Robinson, A. J.; Cotton, J. S.; Ching, C. Y.; Shoukri, M. Electrohydrodynamic enhancement of in-tube convective condensation heat transfer. *Int. J. Heat Mass Transfer* **2006**, *49*, 1647–1657.

(10) Ogata, J.; Yabe, A. Basic study on the enhancement of nucleate boiling heat transfer by applying electric fields. *Int. J. Heat Mass Transfer* **1993**, *36*, 775–782.

(11) Kweon, Y. C.; Kim, M. H. Experimental study on nucleate boiling enhancement and bubble dynamic behavior in saturated pool boiling using a nonuniform dc electric field. *Int. J. Multiphase Flow* **2000**, *26*, 1351–1368.

(12) Wang, P.; Lewin, P. L.; Swaffield, D. J.; Chen, G. Electric field effects on boiling heat transfer of liquid nitrogen. *Cryogenics* **2009**, *49*, 379–389.

(13) McGranaghan, G.; Robinson, A. J. EHD Augmented Convective Boiling: Flow Regimes and Enhanced Heat Transfer. *Heat Transfer Eng.* **2014**, *35*, 517–527.

(14) Kasayapanand, N. Numerical study of electrode bank enhanced heat transfer. *Appl. Therm. Eng.* **2006**, *26*, 1471–1480.

(15) Kasayapanand, N. Electrode arrangement effect on natural convection. *Energy Convers. Manage.* **2007**, *48*, 1323–1330.

(16) Kasayapanand, N. Numerical modeling of the effect of number of electrodes on natural convection in an EHD fluid. *J. Electrost.* **2007**, *65*, 465–474.

(17) Kasayapanand, N. Numerical modeling of natural convection in partially open square cavities under electric field. *Int. Commun. Heat Mass Transfer* **2007**, *34*, 630–643.

(18) Shakouri Pour, M.; Esmaeilzadeh, E. Experimental investigation of convective heat transfer enhancement from 3D-shape heat sources by EHD actuator in duct flow. *Exp. Therm. Fluid Sci.* **2011**, *35*, 1383–1391.

(19) Baghaei Lakeh, R.; Molki, M. Targeted heat transfer augmentation in circular tubes using a corona jet. *J. Electrost.* **2012**, *70*, 31–42.

(20) Baghaei Lakeh, R.; Molki, M. Enhancement of convective heat transfer by electrically-induced swirling effect in laminar and fully-developed internal flows. *J. Electrost.* **2013**, *71*, 1086–1099.

(21) Deylami, H. M.; Amanifard, N.; Dolati, F.; Kouhikamali, R.; Mostajiri, K. Numerical investigation of using various electrode arrangements for amplifying the EHD enhanced heat transfer in a smooth channel. *J. Electrost.* **2013**, *71*, 656–665.

(22) Nahavandi, M.; Mehrabani-Zeinabad, A. Numerical simulation of electrohydrodynamic effect on natural convection through a vertical enclosure channel. *Asia-Pac. J. Chem. Eng.* **2013**, *8*, 756–766.

(23) Robinson, F. N. H. *Macroscopic Electromagnetism*; Pergamon Press: Oxford, U.K., 1973.

(24) Lakeh, R. B.; Molki, M. Patterns of secondary flow field in a circular tube caused by corona wind using the method of characteristics. *Proc. ASME Int. Mech. Eng. Congr. Expos.* Lake Buena Vista, FL, November 13–19, 2009; Vol. 9; 663–671.

(25) Schaub, G.; Unruh, D.; Wang, J.; Turek, T. Kinetic analysis of selective catalytic NO<sub>x</sub> reduction (SCR) in a catalytic filter. *Chem. Eng. Process.* **2003**, *42*, 365–371.

(26) Seong, H. J. *Selective Catalytic Reduction (SCR) of NO by NH<sub>3</sub> in a Fixed-bed Reactor*. M.S. Dissertation, The Pennsylvania State University, State College, PA, 2012.

(27) Nayfeh, M. H.; Brussel, M. K. *Electricity and Magnetism*; Wiley: New York, 1985.

(28) Gordon, S.; McBride, B. J. *Computer program for calculation of complex chemical equilibrium compositions*; NASA: 1972.

(29) Extracted data from the GRI-Mech 3.0, <http://www.me.berkeley.edu/gri-mech/>.

(30) Dhanushkodi, S. R.; Mahinpey, N.; Wilson, M. Kinetic and 2D reactor modeling for simulation of the catalytic reduction of NO<sub>x</sub> in the monolith honeycomb reactor. *Process Saf. Environ. Prot.* **2008**, *86*, 303–309.

(31) Davis, T. A. *Umfpack version 4.4 user guide*; Department of Computer and Information Science and Engineering, University of Florida: Gainesville, FL, 2005.

(32) Saracco, G.; Specchia, V. Catalytic filters for flue-gas cleaning. In *Structured Catalysts and Reactors*; Cybulski, A., Mouljin, J. A., Eds.; Marcel Dekker: New York, 1998; 417–434.

(33) Lintz, H. G.; Turek, T. Intrinsic kinetics of nitric oxide reduction by ammonia on a vanadia-titania catalyst. *Appl. Catal., A* **1992**, *85*, 13–25.

(34) Borisova, E. S.; Noskov, A. S.; Bobrova, L. N. Effect of unsteady-state catalyst surface on the SCR-process. *Catal. Today* **1997**, *38*, 97–105.

(35) Nova, I.; Lietti, L.; Tronconi, E.; Forzatti, P. Dynamics of SCR reaction over a TiO<sub>2</sub>-supported vanadia–tungsta commercial catalyst. *Catal. Today* **2000**, *60*, 73–82.

(36) Hubner, K.; Pape, A.; Weber, E. A. Simultaneous removal of gaseous and particulate components from gases by catalytically activated ceramic filters. *Conf. Proc. High Temp. Gas Cleaning* **1996**, *1*, 267–277.

(37) Debye length. [http://www.soft-matter.seas.harvard.edu/index.php/Debye\\_length](http://www.soft-matter.seas.harvard.edu/index.php/Debye_length).

(38) Eliezer, S.; Eliezer, Y. *The Fourth State of Matter: An Introduction to Plasma Science*; CRC Press: Boca Raton, FL, 2001.

(39) Cheng, D. K. *Field and Wave Electromagnetics*; Addison-Wesley: New York, 1989; Vol. 2.